



Dirichlet Process Clustering-based Radio SLAM with Arbitrarily-Shaped Reflectors

Downloaded from: <https://research.chalmers.se>, 2024-03-20 11:35 UTC

Citation for the original published paper (version of record):

Lee, J., Kim, H., Wymeersch, H. et al (2023). Dirichlet Process Clustering-based Radio SLAM with Arbitrarily-Shaped Reflectors. 2023 IEEE 3rd International Symposium on Joint Communications and Sensing, JC and S 2023. <http://dx.doi.org/10.1109/JCS57290.2023.10107464>

N.B. When citing this work, cite the original published paper.

© 2023 IEEE. Personal use of this material is permitted. Permission from IEEE must be obtained for all other uses, in any current or future media, including reprinting/republishing this material for advertising or promotional purposes, or reuse of any copyrighted component of this work in other works.

Dirichlet Process Clustering-based Radio SLAM with Arbitrarily-Shaped Reflectors

Jaebok Lee*, Hyowon Kim[†], Henk Wymeersch[†], and Sunwoo Kim*,

*Department of Electronic Engineering, Hanyang University, Seoul, Korea

[†]Department of Electrical Engineering, Chalmers University of Technology, Sweden

Abstract—This paper proposes a Dirichlet process (DP)-based radio simultaneous localization and mapping (SLAM) algorithm enabling mapping arbitrary structures (ASs) as well as the standard point landmarks. The ASs cannot be characterized by a low-dimensional state, in contrast to the standard point landmarks, leading to incorrect mapping results in the existing radio SLAM methods. To tackle the incorrect mapping issue, we develop a DP-based data association method, where the landmarks are maintained by the clusters, and each birth point by the measurement is assigned to the existing or a new cluster. Compared to the well-known state-of-the-art method, we evaluate the performance of the proposed algorithm under the scenario with multiple landmarks deployed. This validation represents that radio SLAM is possible in an environment where objects of ASs exist through the proposed method.

Index Terms—5G millimeter wave, 6G Terahertz, simultaneous localization and mapping, Dirichlet process, vehicular networks.

I. INTRODUCTION

In B5G/6G systems, the utilization of higher frequency from mmWave to terahertz (THz) with wider bandwidth and large antenna arrays makes it possible to obtain highly resolvable channel parameters in the time and angular domains [1]. B5G/6G systems also achieve Tbit/s communication rates. Consequently, this has given rise to the concept of integrated sensing and communication (ISAC). ISAC analyzes radio wave transmission, reflection, and scattering to enable the provision of a wider range of new services, including radio simultaneous localization and mapping (SLAM) [2].

In the radio SLAM literature, the random finite set (RFS)-based works have been developed in [3]–[5], where landmark states and their cardinality are modeled as an RFS. The authors in [3] modeled the map as an RFS and the first-order moment (i.e., probability hypothesis density (PHD)) of the set of landmarks is propagated for mapping. To handle the complexity issue of [3], the SLAM filter is jointly implemented by the cubature Kalman filter [6] in [4]. The RFS-based method can lead to formulating the SLAM problem in an optimal manner [5].

The belief propagation (BP)-based radio SLAM methods [7]–[10] have a balanced trade-off between the per-

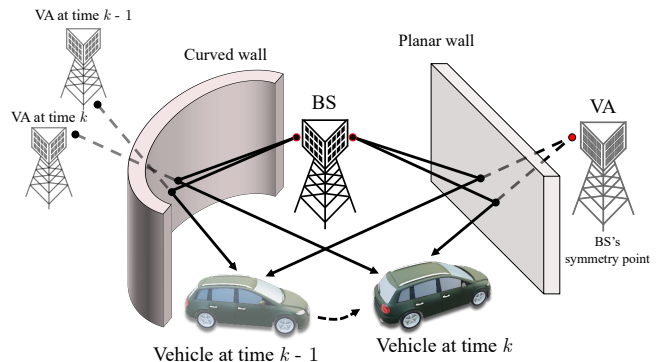


Fig. 1. Illustration of radio signal propagation by the arbitrarily shaped and planar walls. The planar wall can be characterized by a fixed point, while the curved wall cannot.

formance and the computational complexity. In BP-based SLAM method, the landmark is modeled by a vector. The data association process is explicitly handled in the methods of [7], [8], and only planar walls are considered in [7] while the multiple landmark types (including SPs) are addressed in [8]. The joint SLAM density is formulated and marginal posterior densities are computed by BP in [9], and the angle information is used as the additional measurement in [10].

In the existing radio SLAM methods, the standard point landmarks, such as either the planar walls, characterized by the virtual anchor (VAs) or scattering point (SPs), have been considered. However, non-planar walls (e.g., arbitrarily-shaped walls) have not been properly handled, leading to mapping performance degradation due to missed detections or false alarms, as illustrated in Fig. 1.

To tackle the arbitrarily-shaped wall issue, we employ the Dirichlet process (DP) clustering approach in vision-SLAM. We consider that the radio SLAM in B5G/6G resembles to the vision-SLAM as the radio signal paths are getting sparse due to the higher carrier frequency and the radio signals are considered as light. The Dirichlet process (DP), a non-parametric clustering technique, is also suitable for radio SLAM scenarios with limited information of prior knowledge of landmarks, where the radio signals convey geometric information with false alarms and missed detections. Several authors in [11]–[15] have proposed DP-based SLAM and tracking technologies with the vision-based measurements.

This paper is the first attempt to using the DP approach

This work was supported, in part, by Institute of Information & communications Technology Planning & Evaluation (IITP) grant funded by the Korea government (MSIT) (No. 2018-0-01659, 5G Open Intelligence-Defined RAN (ID-RAN) Technique based on 5G New Radio), and Basic Science Research Program through the National Research Foundation of Korea funded by the Ministry of Education (NRF-2022R1A6A3A03068510).

for detecting arbitrarily-shaped walls in radio SLAM scenarios. We propose a DP-based radio SLAM filter, enabling mapping arbitrary structures (ASs) as well as the standard point landmarks. For properly detecting ASs, we develop a DP-based data association method, where the landmarks are maintained by the clusters, and each birth point by the measurement is assigned to the existing or a new cluster. Extensive simulations are carried out to show the superiority of the proposed method in detecting and classifying ASs, compared to the known state-of-the-art method.

II. SYSTEM MODELS

A. Vehicle State and Dynamics

We denote a vehicle state at time k by $\mathbf{s}_k = [\mathbf{x}_{k,s}^\top, \alpha_k, \zeta_k, \xi_k, B_k]^\top \in \mathbb{R}^7$, where $\mathbf{x}_{k,s} = [x_{k,s}, y_{k,s}, z_{k,s}]^\top$, α_k, ζ_k, ξ_k , and B_k are 3-dimensional position, heading, translation speed, turn-rate, and clock bias. With the known transition density $f(\mathbf{s}_k|\mathbf{s}_{k-1})$, the vehicle dynamics follow the motion model [16, Chapter 5]:

$$\mathbf{s}_k = \mathbf{g}(\mathbf{s}_{k-1}) + \mathbf{q}_k, \quad (1)$$

where $\mathbf{g}(\cdot)$ is the known transition function, and \mathbf{q}_k denotes the process noise, modeled as the zero-mean Gaussian distribution with the known covariance \mathbf{Q} .

B. Propagation Environment

The propagation environment is specified by the following four types of landmarks: i) a single BS, periodically transmitting mmWave signals; ii) large planar walls which specularly reflect the signal, each is characterized as one VA; iii) small objects (*i.e.*, SPs) that scatter the signals; and iv) arbitrarily-shaped walls, which specularly reflect the signal at the incident point on the wall.

A landmark location is denoted by $\mathbf{x}_m \in \mathbb{R}^3$, and a landmark type is represented by $m \in \mathcal{M}$, where $\mathcal{M} = \{\text{BS}, \text{VA}, \text{SP}, \text{AS}\}$. A static BS location, denoted by $\mathbf{x}_{\text{BS}} \in \mathbb{R}^3$, is known. We denote VA and SP locations by \mathbf{x}_{VA} and \mathbf{x}_{SP} , respectively, also static. While the VAs and SPs are modeled as the standard fixed points, the ASs are modeled as a collection of time-varying incident points.

C. Observation

At time k , the BS transmits the mmWave/THz signals, and the vehicle receives multipath consisting of LOS and NLOS paths. Among the resolvable signal paths, we consider a LOS path (BS to vehicle) and single-bounce NLOS paths (BS to reflector to vehicle and BS to SP to vehicle), due to the severe path loss. We assume other paths cannot be detectable due to severe signal attenuation. After the channel estimation routine [17] at the receiver, the vehicle obtains the measurements. The signal path is indexed by i , and the measurement of signal path i is denoted by \mathbf{z}_k^i . A set of measurements is denoted by $\mathcal{Z}_k = \{\mathbf{z}_k^1, \dots, \mathbf{z}_k^{I_k}\}$. Following [3], the measurement \mathbf{z}_k^i for each path is modeled as

$$\mathbf{z}_k^i = h(\mathbf{s}_k, \mathbf{x}^i, m) + \mathbf{n}_{k,m}^i, \quad (2)$$

where $h(\mathbf{s}_k, \mathbf{x}^i, m) = [\tau_k^i, (\boldsymbol{\theta}_k^i)^\top, (\boldsymbol{\phi}_k^i)^\top]^\top$, $\mathbf{n}_{k,m}^i \sim \mathcal{N}(\mathbf{0}, \mathbf{N}_m)$ with the covariance matrix \mathbf{N}_m . Here, $\tau_k^i, \boldsymbol{\theta}_k^i = [\theta_{k,az}^i, \theta_{k,el}^i]^\top$, and $\boldsymbol{\phi}_k^i = [\phi_{k,az}^i, \phi_{k,el}^i]^\top$ respectively denote the time of arrival (TOA), direction of arrival (DOA) in azimuth and elevation, and direction of departure (DOD) in azimuth and elevation. Due to the channel estimation error, false alarm, transient vehicle, or object that is only visible during a short time, may occur, considered as clutter. The clutter measurement is included in \mathcal{Z}_k with the element \mathbf{z}_k^i .

III. METHODOLOGY FOR DIRICHLET PROCESS-BASED SIMULTANEOUS LOCALIZATION AND MAPPING

A. Vehicle Prediction

Given the posterior density of the vehicle state at time $k-1$, $f(\mathbf{s}_{k-1}|\mathcal{Z}_{1:k-1}) = \mathcal{N}(\mathbf{s}_{k-1}; \bar{\mathbf{s}}_{k-1}, \tilde{\mathbf{V}}_{k-1})$, where $\bar{\mathbf{s}}_{k-1}, \tilde{\mathbf{V}}_{k-1}$ are the mean and covariance of predicted vehicle state at time $k-1$, respectively. The predicted vehicle density at time k is denoted by $f(\mathbf{s}_k|\mathcal{Z}_{1:k-1}) = \mathcal{N}(\mathbf{s}_k; \bar{\mathbf{s}}_k, \bar{\mathbf{V}}_k)$, is given by

$$f(\mathbf{s}_k|\mathcal{Z}_{1:k-1}) = \int f(\mathbf{s}_k|\mathbf{s}_{k-1})f(\mathbf{s}_{k-1}|\mathcal{Z}_{1:k-1})d\mathbf{s}_{k-1}. \quad (3)$$

We compute the mean $\bar{\mathbf{s}}_k$ and covariance $\bar{\mathbf{V}}_k$ as

$$\bar{\mathbf{s}}_k = \mathbf{g}(\mathbf{s}_{k-1}), \quad (4)$$

$$\bar{\mathbf{V}}_k = \mathbf{G}_k \tilde{\mathbf{V}}_{k-1} \mathbf{G}_k^\top + \mathbf{Q}, \quad (5)$$

where \mathbf{G}_k is a Jacobian matrix of $\mathbf{g}(\cdot)$, with $\partial \mathbf{g}(\mathbf{s}_{k-1})/\partial \mathbf{s}_{k-1}$.

B. Environmental Mapping using DP Clustering

The proposed DP-based mapping process consists of the birth generation and clustering.

1) *Initialization*: In the initial step ($k = 1$), the map is empty. When $k > 1$, the prior map is given with the following components: cluster mean $\mathbf{c}_{k-1,m}^j$, cluster covariance $\boldsymbol{\Sigma}_{k-1,m}^j$, and the number of data points that consists of the corresponding cluster $d_{k-1,m}^j$ of the j -th cluster whose type is m at time $k-1$.

2) *Birth Generation Process*: In the birth process, the birth point for landmark type m by the measurement \mathbf{z}_k^i is denoted by $\mathbf{b}_{k,m}^i$, modeled as the Gaussian density:

$$\mathbf{b}_{k,m}^i \sim \mathcal{N}(\mathbf{m}_{k,m}^i, \mathbf{C}_{k,m}^i), \quad (6)$$

where $\mathbf{m}_{k,m}^i$ and $\mathbf{C}_{k,m}^i$ are respectively the birth mean and covariance. The computation of $\mathbf{m}_{k,m}^i$ and $\mathbf{C}_{k,m}^i$ is detailed in [3, Appendix B]. We employ the same birth generation procedure for AS birth points as for SP.

3) *Data Association with DP Clustering*: In parallel, each generated birth will go through the following process.

a) *VA & SP Mapping*: For VA mapping, we calculate and compare the probability that each birth point belongs to the existing and new clusters ($m = \text{VA}$). The probabilities of i -th birth point $\mathbf{b}_{k,m}^i$ will be included in existing $J_{k-1,m}$ clusters, and a new cluster, referred as $(J_{k-1,m}+1)$ -th cluster at time k are expressed as follows respectively.

- Existing cluster ($j \leq J_{k-1,m}$)

$$p(l_i = j | \mathbf{l}_{-i}, \omega) = \mathcal{N}(\mathbf{m}_{k,m}^i; \mathbf{c}_{k-1,m}^j, \Sigma_{k-1,m}^j) \frac{d_{k-1,m}^j}{D_k - 1 + \omega}, \quad (7)$$

- New cluster ($j = J_{k-1,m} + 1$)

$$p(l_i = j | \mathbf{l}_{-i}, \omega) = \mathcal{N}(\mathbf{m}_{k,m}^i; \mathbf{c}^0, \Sigma^0) \frac{\omega}{D_{k,m} - 1 + \omega}, \quad (8)$$

where j is the cluster index, $J_{k-1,m}$ is the number of the existing clusters of type m . $l_i \in \mathcal{L}_i$ denotes the association variable, where $\mathcal{L}_i = \{1, \dots, J_{k-1,m} + 1\}$, and $\mathbf{l}_{-i} = \mathcal{L}_i \setminus \{l_i\}$. Note that \mathbf{c}^0 and Σ^0 are the mean and covariance of the 0-th cluster, which is defined by a new cluster created due to data points that does not belong to any existing cluster. ω is the concentration parameter of DP, and $D_{k,m} = \sum_j d_{k-1,m}^j + 1$ indicates the total number of new data points and stacked data points consisting of type m 's clusters up to time $k-1$. We compare these probabilities and decide that the data points belong to the cluster with the highest probability j_i^* as follows.

$$j_i^* = \underset{j \in \{1, \dots, J_{k-1,m} + 1\}}{\operatorname{argmax}} p(l_i = j). \quad (9)$$

Now, the birth $\mathbf{b}_{k,m}^i$ in (6) is assigned to the j_i^* -th cluster with type m . We set $d_{k,m}^{j_i^*} = d_{k-1,m}^{j_i^*} + 1$ for $j_i^* \leq J_{k-1,m}$, and for $j_i^* = J_{k-1,m} + 1$, $d_{k,m}^{j_i^*} = 1$. The following clusters are determined as the landmark with type m : $d_{k,m}^{j_i^*} \geq N_m$, where N_m is the threshold for detection of landmark with type m .

After the VA mapping is finished, the SP mapping starts with the measurements that were assigned to either $j_i^* = J_{k-1,VA} + 1$ or $j_i^* \leq J_{k-1,VA}$ with $d_{k,VA}^{j_i^*} < N_{VA}$, performed in parallel, as VA mapping above.

b) AS mapping: Unlike the previous point-shaped distributed VA/SP mapping, another method is required to map AS distributed along with the shape of an object. To cluster the AS, we set the AS cluster as a Gaussian mixture consisting of the points with mean and covariance assigned to the cluster. We denote the mean and covariance of ϵ -th data points of j -th AS cluster at time k by $\mathbf{d}_{k,AS}^{\epsilon,j}$ and $\mathbf{D}_{k,AS}^{\epsilon,j}$, respectively. Therefore, the probability that birth points belong to each cluster can be obtained as follows.

- Existing cluster ($j \leq J_{k-1,AS}$)

$$p(l_i = j | \mathbf{l}_{-i}, \omega) = \sum_{\epsilon=1}^{d_{k,AS}^j} \mathcal{N}(\mathbf{m}_{k,AS}^i; \mathbf{d}_{k-1,AS}^{\epsilon,j}, \mathbf{D}_{k-1,AS}^{\epsilon,j}) \frac{d_{k-1,AS}^j}{E_k - 1 + \omega}, \quad (10)$$

- New cluster ($j = J_{k-1,AS} + 1$)

$$p(l_i = j | \mathbf{l}_{-i}, \omega) = \mathcal{N}(\mathbf{m}_{k,AS}^i; \mathbf{c}^0, \Sigma^0) \frac{\omega}{E_k - 1 + \omega}, \quad (11)$$

where $E_k = \sum_j d_{k-1,AS}^j + 1$ indicates the total number of new data points and stacked data points consisting of AS clusters up to time $k-1$. Finally, in the same way, as in (9), the final cluster to which the birth point belongs is determined. The following clusters are determined as AS: $d_{k,AS}^j \geq N_{AS}$.

At the end of this environment mapping, all birth points are assigned to the clusters. Then, we can obtain the cluster indices that the birth points are assigned, different from j_i^* in (9), as follows: $q(i)^* = j_m$ for $i \in \mathcal{I}_k = \{i : d_{k,m}^{j_i^*} \geq N_m \text{ for } m = \{VA, SP\}\}$, indicating that the measurement \mathbf{z}_k^i generates the birth point $\mathbf{b}_{k,m}^i$ for the landmark types, and the birth $\mathbf{b}_{k,m}^i$ is assigned to the cluster j with the landmark type m . For example, when $q(2) = 3_{VA}$, then $\mathbf{c}_{k-1}^{q(2)} = \mathbf{c}_{k-1,VA}^3$ and $\Sigma_{k-1}^{q(2)} = \Sigma_{k-1,VA}^3$. Note that the clusters that had been determined as landmarks at least once (by $d_{k',m}^{j_i^*} \geq N_m$ for $k' < k$) remain as landmarks even if no birth point is assigned at time k .

C. Map Update by DP Cluster

Given the data association with the assigned birth points, we update the VA and SP clusters. For the assigned birth point $\mathbf{b}_{k,m}^i$ and assigned cluster index j_i^* , we update the cluster covariance $\Sigma_{k,m}^{j_i^*}$ and mean $\mathbf{c}_{k,m}^{j_i^*}$ as follows [18]:

$$\begin{aligned} \Sigma_{k,m}^{j_i^*} &= ((\Sigma_{k-1,m}^{j_i^*})^{-1} + (\mathbf{C}_{k,m}^i)^{-1})^{-1}, \\ \mathbf{c}_{k,m}^{j_i^*} &= \Sigma_{k,m}^{j_i^*} ((\Sigma_{k-1,m}^{j_i^*})^{-1} \mathbf{c}_{k-1,m}^{j_i^*} + (\mathbf{C}_{k,m}^i)^{-1} \mathbf{m}_{k,m}^i). \end{aligned} \quad (12)$$

When the birth point is assigned to a new cluster, we set the mean $\mathbf{c}_{k,m}^{j_i^*} = \mathbf{m}_{k,m}^i$ and covariance $\Sigma_{k,m}^{j_i^*} = \mathbf{C}_{k,m}^i$.

D. Vehicle Update

To update the vehicle state, instead of using the particle filter we estimate the posterior of joint vehicle state and detected landmarks density, and the detected landmarks are marginalized out. At the end of data association, the cluster indices $q(i)$ returned $|\mathcal{I}_k|$ landmarks, where $|\cdot|$ stands for the set cardinality, and we introduce the random vector for joint vehicle and detected landmarks

$$\mathbf{t}_k = [(\mathbf{s}_k)^\top, \dots, (\mathbf{x}_k^{|\mathcal{I}_k|})^\top]^\top, \quad (14)$$

with an a priori Gaussian distribution $\mathcal{N}(\mathbf{t}_k, \bar{\mathbf{t}}_k, \bar{\mathbf{T}}_k)$, where

$$\bar{\mathbf{t}}_k = [(\bar{\mathbf{s}}_k)^\top, \dots, (\bar{\mathbf{c}}_k^{q(\mathcal{I}_k)})^\top]^\top, \quad (15)$$

$$\bar{\mathbf{T}}_k = \text{blkdiag}(\bar{\mathbf{V}}_k, \dots, \Sigma_k^{q(\mathcal{I}_k)}), \quad (16)$$

where $\text{blkdiag}(\cdot)$ is the block diagonalizing function. We recall that the following example of data association and corresponding cluster: when $q(2) = 3_{VA}$, then $\mathbf{c}_{k-1}^{q(2)} = \mathbf{c}_{k-1,VA}^3$ and $\Sigma_{k-1}^{q(2)} = \Sigma_{k-1,VA}^3$. Given the corresponding measurements to the detected landmarks $\mathbf{z}_k = [\mathbf{z}_k^1, \dots, \mathbf{z}_k^{|\mathcal{I}_k|}]^\top$, we estimate the joint posterior density of the vehicle state and detected landmarks, approximated to the Gaussian distribution by the standard extended Kalman filter [19].

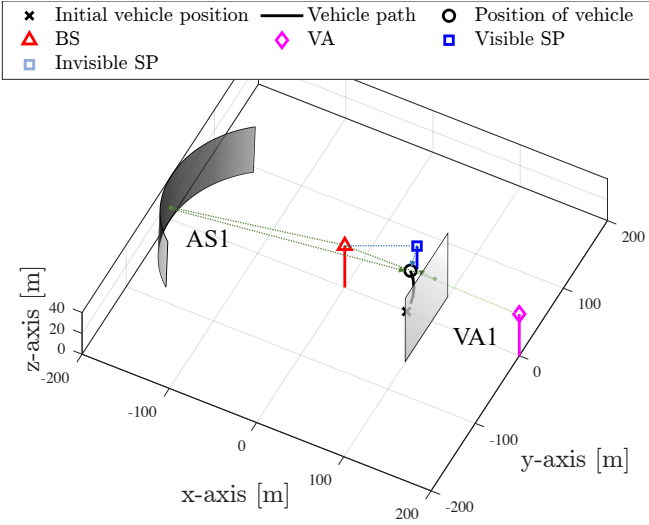


Fig. 2. Examples of propagation environments caused by VA, SP, and AS. The simulation environment includes 1 vehicle, 1 BS, 1 VA, 1 SP, and 1 AS.

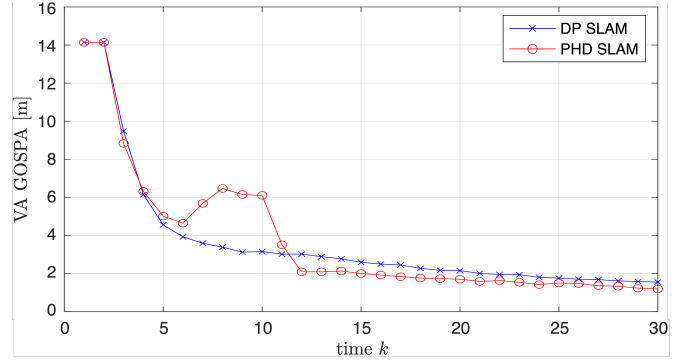
TABLE I
SIMULATION PARAMETER UNITS

Parameter	Units
$\text{diag}(\mathbf{Q})$	$[\text{m}^2, \text{m}^2, \text{m}^2, \text{rad}^2, \text{rad}^2, \text{rad}^2, \text{rad}^2]$
\mathbf{s}_0, σ_0	$[\text{m}, \text{m}, \text{m}, \text{rad}, \text{m/s}, \text{rad/s}, \text{m}]^\top$
$\text{diag}(\mathbf{N})$	$[\text{m}^2, \text{rad}^2, \text{rad}^2, \text{rad}^2, \text{rad}^2]$
$\text{diag}(\Sigma), \text{diag}(\Sigma_0)$	$[\text{m}, \text{m}]$
μ_0	$[\text{m}, \text{m}, \text{m}]$

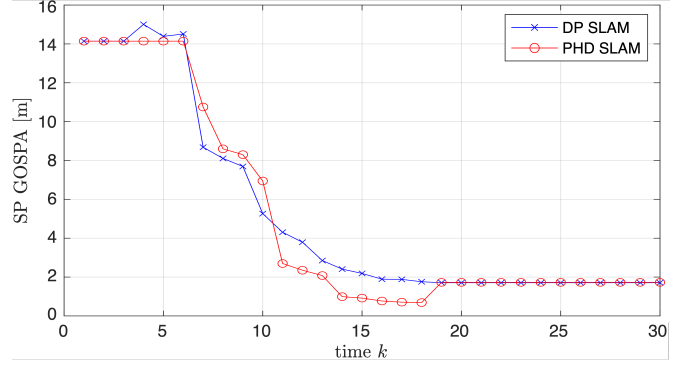
IV. PERFORMANCE EVALUATION

A. Simulation Environment

We consider a vehicle that drives along a circular road for $K_{\max} = 30$ with an interval of 0.5 seconds. The MATLAB simulation is conducted using the parameters as follows. We set \mathbf{Q} , the covariance noise matrix as $\text{diag}[0.2^2, 0.2^2, 0, 0.01^2, 0, 0, 0.2^2]$. The initial state of the vehicle was set as $\mathbf{s}_0 = [0.7285, 0, 0, \pi/2, 22.22, 2\pi/15, 300]^\top$ and assume that the translation speed and turn-rate are known. The initial prior of the vehicle state follows Gaussian distribution with the standard deviation $\sigma_0 = [0.3, 0.3, 0, 0.3, 0, 0, 0.3]^\top$. We set \mathbf{N}_m differently depending on the object, for $m = \text{BS}, \text{VA}$, $\mathbf{N}_m = \text{diag}[0.1, 0.01, 0.01, 0.01, 0.01]$ and for $m = \text{SP}, \text{AS}$, $\mathbf{N}_m = 2\mathbf{N}_{\text{VA}}$. For DP, we set ω , μ_0 , and Σ^0 as 0.9, $[0, 0, 0]^\top$, and $\text{diag}[100, 100, 100]$ respectively, and the units of simulation parameters are listed in Table I. The thresholds for the clusters to be determined as the detected landmarks of VA, SP, and AS are respectively denoted by N_{VA} , N_{SP} , and N_{AS} , set to 3, 3, and 5. As shown in Fig. 2, the BS is located at $[0, 0, 40]^\top$, and a VA is located at $[200, 0, 40]^\top$, with unit m. A SP is located at $[65, 65, z_{\text{SP}}]^\top$ with unit m and $z_{\text{SP}} \sim \mathcal{U}(0, 40)$. For AS, we place a cylindrical wall with a center of $[-100, 0]^\top$ and a radius of 100 on the xy plane with



(a)



(b)

Fig. 3. Average GOSPA of (a) VA and (b) SP by the proposed method. SP is detected in turn due to the limited FoV, and the SP GOSPA decreases stepwise (2 steps).

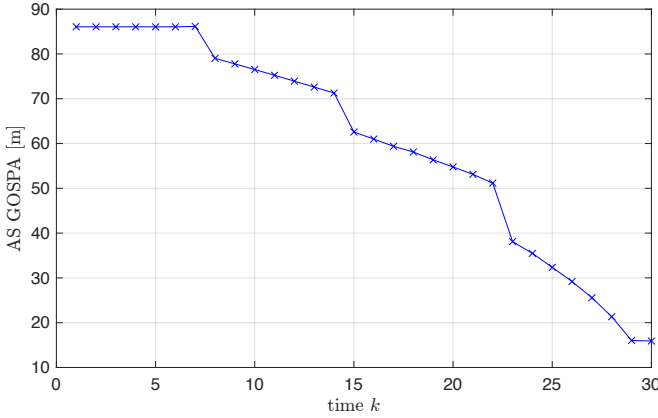
unit m. The face of AS is the concave face of the cylinder when viewed from the BS.

We set the detection probability, $p_D = 0.9$ within the field of view (FoV). The FoV of signal from SP and AS is 50 m, and from BS and VA is always visible. We consider clutter intensity, $c(\mathbf{z})$ follows Poisson distribution as $\lambda/(4R_{\max}\pi^4)$ as the average of the number of clutter measurements $\lambda = 1$, and the maximum sensing range $R_{\max} = 100$ m. We use the average of the generalized optimal subpattern assignment (GOSPA) distance [20] for measuring the mapping performance, and the parameter settings as [3] for calculating GOSPA distance were used. Simulation results are obtained by averaging over 100 Monte Carlo runs and using MATLAB implementation for the proposed SLAM algorithm, executed on a PC with 3.2 GHz M1 pro CPU and 16 GB RAM, and the OS is macOS Monterey.

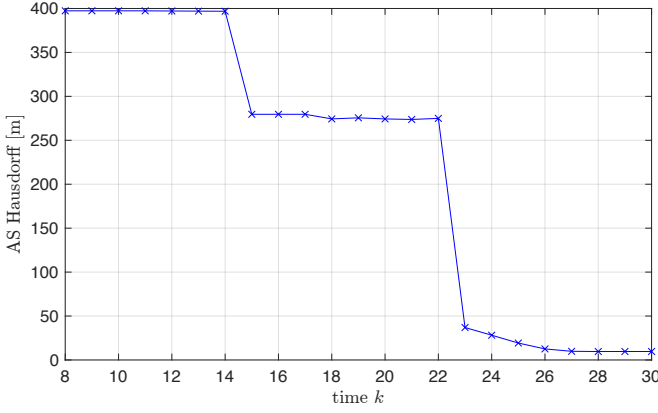
B. Simulation Results

Under the above simulation environment, we evaluate the performance of the proposed algorithm. The mapping performance for VA, SP, and AS is evaluated by the GOSPA distance, and the vehicle localization performance by the root means square error (RMSE).

1) *Mapping*: Fig. 3 represents the mapping performance for VAs and SPs of the proposed SLAM filter, compared to PHD SLAM [3]. In the case of the VA, Fig. 3(a) shows



(a)



(b)

Fig. 4. Mapping performance of AS, (a) average GOSPA, (b) Hausdorff distance by the proposed method. GOSPA decreases in stages, and the rate of decrease is relatively slow because many points can be detected.

the average GOSPA of VAs. The GOSPA of the proposed method is lower than that of [3] across all time steps except for a few time steps. In particular, in the case of PHD SLAM, prominent peaks occur over the entire period. This is because the PHD-SLAM filter does not correctly capture the ASs and regards them as VAs. On the other hand, AS measurements are well addressed in the proposed SLAM filter due to the developed DP-based data association method. Fig. 3(b) shows the average GOSPA distances for SPs. Because of the limited FoV of the vehicle, the SP is detected only at a specific time to the vehicle. From $k = 7$, the SPs are getting detectable, and the GOSPA distance of SPs sharply decrease. After $k = 18$, the gap of two GOSPA distances between the proposed and PHD-SLAM filter is about 0.01 m.

Unlike the above two types of landmarks, each AS is not expressed as one fixed point. Therefore, we calculated the AS GOSPA distances by assuming that the set of incident points on the arbitrary-shaped wall is the ground-truth. Fig. 4(a) shows the AS GOSPA of the proposed SLAM filter. Due to the relatively larger number of points to be detected in ASs than that of VAs and SPs, the AS GOSPA distance at $k = 1$ is larger than the VA and SP GOSPA distances. As the ASs are

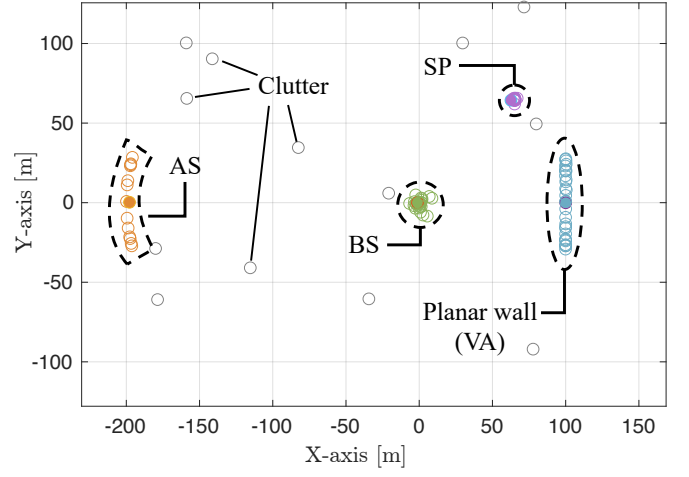


Fig. 5. Mapping results employing the proposed DP SLAM in the environment of Fig. 2. VA, SP, and AS were mapped, and clutter was distinguished by the proposed method.

detected over time steps, the AS GOSPA distance gradually decrease. For another AS mapping performance metric, we use the Hausdorff distances, widely used to evaluate the image matching performance by comparing the images [21]. Assume a set of points at actual locations, \mathcal{A} , and a set of estimated points, \mathcal{B} , composed of discrete points. The Hausdorff distance $H(\mathcal{A}, \mathcal{B})$ is defined as

$$H(\mathcal{A}, \mathcal{B}) = \max(h(\mathcal{A}, \mathcal{B}), h(\mathcal{B}, \mathcal{A})), \quad (17)$$

where $h(\mathcal{A}, \mathcal{B}) = \max_{a \in \mathcal{A}} \min_{b \in \mathcal{B}} \|a - b\|$. We set \mathcal{A} to the ground-truth for ASs: incident points on the arbitrary-shaped wall and \mathcal{B} to the determined ASs. Fig. 4(b) shows the average Hausdorff distance of ASs, which also gradually decrease as the ASs are determined over time steps.

Fig. 5 illustrates the mapping results by the proposed DP-SLAM filter, where the small circles with the same color are recognized as a single cluster. The green, blue, purple, and orange circles represent a BS, a planar wall, a SP, and an arbitrary-shaped wall, respectively. Each gray circle represents clutter that has never belonged to any cluster and were not determined as the detected landmarks.

2) *Localization*: Fig. 6 shows the RMSEs of the vehicle location of the proposed and PHD-SLAM filters. Due to the fact that the vehicle and map are correlated and there are false alarms in the VA map, the localization performance by the proposed SLAM filter is better than the PHD-SLAM filter.

3) *Complexity*: Furthermore, we confirm that there is a distinct gain in the complexity. For Rao-Blackwellized particle filtering in the PHD filter [3], 2000 particle samples are used. The average operation time consumed by the proposed algorithm is 3.5 seconds per 1 Monte Carlo simulation run, whereas the PHD-SLAM filter [3] consumes more than 8000 seconds.

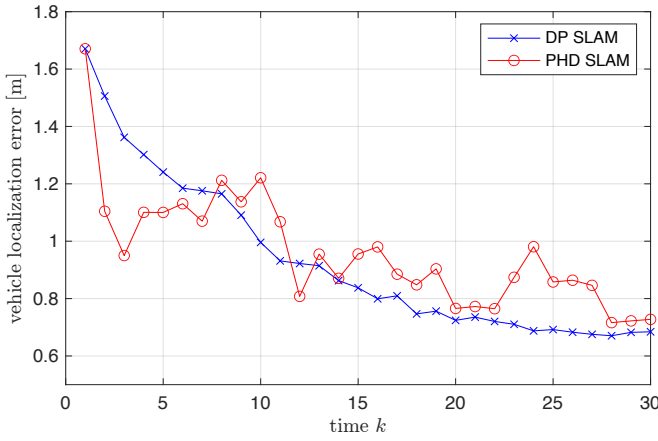


Fig. 6. RMSEs of vehicle location estimates by the proposed method compared to [3].

V. CONCLUSIONS

In this paper, we have proposed a DP-based radio SLAM filter that can detect arbitrarily-shaped landmarks as well as other standard point landmarks, while the existing radio SLAM filters cannot. Thanks to the developed data association with the DP approach, the birth points by the measurements are assigned to the corresponding cluster, leading to SLAM performance improvement. From the simulation results, we confirmed that the proposed SLAM filter is robust to false alarms and missed detections and can well maintain maps for the different types of landmarks, and provides the satisfactory SLAM performance with the reasonable computational complexity.

REFERENCES

- [1] H. Chen, H. Saeeddeen, T. Ballal, H. Wymeersch, M.-S. Alouini, and T. Y. Al-Naffouri, "A tutorial on terahertz-band localization for 6G communication systems," *IEEE Commun. Surveys Tuts.*, vol. 24, no. 3, pp. 1780–1815, 2022.
- [2] A. Liu, Z. Huang, M. Li, Y. Wan, W. Li, T. X. Han, C. Liu, R. Du, D. K. P. Tan, J. Lu, Y. Shen, F. Colone, and K. Chetty, "A survey on fundamental limits of integrated sensing and communication," *IEEE Commun. Surveys Tuts.*, vol. 24, no. 2, pp. 994–1034, 2022.
- [3] H. Kim, K. Granström, L. Gao, G. Battistelli, S. Kim, and H. Wymeersch, "5G mmWave cooperative positioning and mapping using multi-model PHD filter and map fusion," *IEEE Trans. Wireless Commun.*, vol. 19, no. 6, pp. 3782–3795, 2020.
- [4] H. Kim, K. Granström, S. Kim, and H. Wymeersch, "Low-complexity 5G SLAM with CKF-PHD filter," in *Proc. IEEE Int. Conf. Acoust., Speech, Signal Process. (ICASSP)*, Virtual Conference, May 2020, pp. 5220–5224.
- [5] H. Kim, K. Granström, L. Svensson, S. Kim, and H. Wymeersch, "PMBM-based SLAM filters in 5G mmWave vehicular networks," *IEEE Trans. Veh. Technol.*, vol. 71, no. 8, pp. 8646–8661, Aug. 2022.
- [6] I. Arasaratnam and S. Haykin, "Cubature Kalman filters," *IEEE Trans. Autom. Control*, vol. 54, no. 6, pp. 1254–1269, Jun. 2009.
- [7] H. Wymeersch, N. Garcia, H. Kim, G. Seco-Granados, S. Kim, F. Wen, and M. Fröhle, "5G mmWave downlink vehicular positioning," in *Proc. of IEEE Global Communications Conference (GLOBECOM)*, 2018, pp. 206–212.
- [8] H. Kim, H. Wymeersch, N. Garcia, G. Seco-Granados, and S. Kim, "5G mmWave vehicular tracking," in *Proc. IEEE 52nd Asilomar Conf. Signals, Syst., and Comput.*, 2018, pp. 541–547.
- [9] E. Leitinger, F. Meyer, F. Hlawatsch, K. Witrisal, F. Tufvesson, and M. Z. Win, "A belief propagation algorithm for multipath-based SLAM," *IEEE Trans. Wireless Commun.*, vol. 18, no. 12, pp. 5613–5629, 2019.
- [10] E. Leitinger, S. Grebien, and K. Witrisal, "Multipath-based SLAM exploiting AoA and amplitude information," in *Proc. Int. Conf. Commun. Workshop (ICC)*, 2019, pp. 1–7.
- [11] B. Moraffah, C. Brito, B. Venkatesh, and A. Papandreou-Suppappola, "Use of hierarchical Dirichlet processes to integrate dependent observations from multiple disparate sensors for tracking," in *Proc. 22th Int. Conf. Inf. Fusion (FUSION)*, 2019, pp. 1–7.
- [12] E. B. Fox, E. B. Sudderth, and A. S. Willsky, "Hierarchical Dirichlet processes for tracking maneuvering targets," in *Proc. 10th Int. Conf. Inf. Fusion (FUSION)*, 2007, pp. 1–8.
- [13] X. Sun, N. H. C. Yung, and E. Y. Lam, "Unsupervised tracking with the doubly stochastic Dirichlet process mixture model," *IEEE Trans. Intell. Transp. Syst.*, vol. 17, no. 9, pp. 2594–2599, 2016.
- [14] B. Mu, S. Liu, L. Paull, J. Leonard, and J. P. How, "SLAM with objects using a nonparametric pose graph," in *IEEE/RSSJ Int. Conf. on Intelligent Robots and Systems (IROS)*, 2016, pp. 4602–4609.
- [15] J. Zhang, M. Gui, Q. Wang, R. Liu, J. Xu, and S. Chen, "Hierarchical topic model based object association for semantic SLAM," *IEEE Trans. Vis. Comput. Graph.*, vol. 25, no. 11, pp. 3052–3062, 2019.
- [16] S. Thrun, W. Burgard, and D. Fox, *Probabilistic Robotics (Intelligent Robotics and Autonomous Agents Series)*. Cambridge, MA, USA: MIT Press, 2005.
- [17] Y. Ge, H. Kim, F. Wen, L. Svensson, S. Kim, and H. Wymeersch, "Exploiting diffuse multipath in 5G SLAM," in *Proc. of IEEE Global Communications Conference (GLOBECOM)*, 2020, pp. 1–6.
- [18] K. B. Petersen, M. S. Pedersen *et al.*, "The matrix cookbook," *Technical University of Denmark*, vol. 7, no. 15, p. 510, 2008.
- [19] R. E. Kalman, "A new approach to linear filtering and prediction problems," *ASME J. Basic Eng.*, vol. 82, pp. 34–45, Mar. 1960.
- [20] A. S. Rahmathullah, A. F. García Fernández, and L. Svensson, "Generalized optimal sub-pattern assignment metric," in *Proc. 20th Int. Conf. Inf. Fusion (FUSION)*, 2017, pp. 1–8.
- [21] D. Huttenlocher, G. Klanderman, and W. Rucklidge, "Comparing images using the Hausdorff distance," *IEEE Transactions on Pattern Analysis and Machine Intelligence*, vol. 15, no. 9, pp. 850–863, 1993.